

Heavy polarons in ultracold atomic Fermi superfluids at the BEC-BCS crossover: Formalism and applications

Jia Wang ,* Xia-Ji Liu, and Hui Hu

Centre for Quantum Technology Theory, Swinburne University of Technology, Melbourne 3122, Australia

 (Received 10 February 2022; revised 20 March 2022; accepted 31 March 2022; published 26 April 2022)

We investigate the system of a heavy impurity embedded in a paired two-component Fermi gas at the crossover from a Bose-Einstein condensate (BEC) to a Bardeen-Cooper-Schrieffer (BCS) superfluid via an extension of the functional determinant approach (FDA). FDA is an exact numerical approach applied to study manifestations of Anderson's orthogonality catastrophe (OC) in the system of a static impurity immersed in an ideal Fermi gas. Here, we extend the FDA to a strongly correlated superfluid background described by a BCS mean-field wave function. In contrast to the ideal Fermi gas case, the pairing gap in the BCS superfluid prevents the OC and leads to genuine polaron signals in the spectrum. Thus our exactly solvable model can provide a deeper understanding of polaron physics. In addition, we find that the polaron spectrum can be used to measure the superfluid pairing gap, and in the case of a magnetic impurity, the energy of the subgap Yu-Shiba-Rusinov (YSR) bound state. Our theoretical predictions can be examined with state-of-art cold-atom experiments.

DOI: [10.1103/PhysRevA.105.043320](https://doi.org/10.1103/PhysRevA.105.043320)

I. INTRODUCTION

The dynamics of an impurity interacting with a bath of quantum-mechanical particles are unique and fundamental in understanding many-body quantum physics [1–3]. On the one hand, system's simplicity allows us to develop insightful theoretical models and, in some cases, access exact solutions to make quantitative comparisons with experiments [4,5]. On the other hand, since a single impurity barely affects the background, we can apply the impurity as a sensitive probe of the surrounding many-particle medium [1]. Two important and related theoretical concepts have been developed to study the impurity-medium problems: polarons [2,3] and orthogonality catastrophe (OC) [6,7].

In 1933, Landau [8] introduced the general concept of polarons to describe impurity-medium systems as quasiparticles formed by dressing the impurity with elementary excitations of the medium. Polarons have become some of the most celebrated “quasiparticles” in condensed matter physics and can be commonly found in various crystalline solids [9,10]. In recent years, polaron physics in experiment [11–21] and theory [22–39] has progressed rapidly in the new platform of ultracold quantum gases, which provides unprecedented controllability and accessibility [40,41]. The insightful concept of polaron leads to developing approximate approaches such as the extended Chevy's ansatz [22,26] or the many-body T -matrix method [2,24,36] that includes only a few medium excitations, which proved to be an excellent approximation for mobile impurities. The underlying physics is that multiple

medium excitations cost the mobile impurity's recoil energy and are energetically unfavorable. Together with Monte Carlo simulations, these approximated approaches predict several characteristic features of the polaron spectrum: attractive and repulsive polaron branches with finite residue, the dark continuum [35], and the molecule-hole continuum [2]. While both attractive and repulsive polarons have been observed in experiments [13,14], other features remain elusive due to the uncertainty in theoretical calculations.

In contrast to a mobile impurity, an infinitely heavy impurity immersed in a Fermi sea can excite many particle-hole pairs close to the Fermi surfaces without costing recoil energy, leading to the occurrence of OC [3,7]. The concept of OC, i.e., the many-particle states with and without impurity become orthogonal, was raised by Anderson in 1967 [6] to understand the Fermi-edge singularity of x-ray absorption spectra in metals [4,5]. This well-known Fermi-edge singularity is the first and most important example of nonequilibrium many-body physics and is exactly solvable [42,43] via the functional determinant approach (FDA) [44–47]. Unfortunately, OC leads to vanishing quasiparticle residues [3], where polaron does not technically exist. Consequently, this exactly solvable model may not be directly applied to understand polarons.

The present study, which accompanies the Letter Ref. [48], investigates a heavy impurity immersed in a two-component Fermi superfluid medium described by the standard Bardeen-Cooper-Schrieffer (BCS) pairing theory [49–51]. The purpose is twofold.

First, we aim to construct an exactly solvable model for polaron with finite residue. As shown in this study, our system is suitable for an exact approach—an extended FDA, and the presence of a pairing gap can efficiently suppress multiple particle-hole excitations and prevent Anderson's OC. Therefore our model provides a benchmark calculation of the polaron spectrum and rigorously examine all the speculated polaron features. We name our system “heavy crossover

*Corresponding author: jjawang@swin.edu.au

polaron" since the background Fermi gas can undergo a crossover from a Bose-Einstein condensation (BEC) to a BCS superfluid.

Second, our prediction can be applied to investigate the background Fermi superfluid excitations, a long-standing topic in ultracold atoms. Polarons have already been realized in BEC and ideal Fermi gas experimentally, but the physics of these weakly interacting background gas are well understood. More recently, it has also been shown that polarons in BEC with a synthetic spin-orbit-coupling can reveal the nature of the background roton excitations [38]. Investigating polaron physics in a strongly correlated Fermi superfluid at the BEC-BCS crossover, namely crossover polaron, has also been proposed in several pioneering works with approximated approaches [52–56]. Our exact method in the heavy impurity limit allows us to apply the polaron spectrum to measure the Fermi superfluid excitation features such as the pairing gap and subgap Yu-Shiba-Rusinov (YSR) bound states [57–61], which is highly experimentally relevant. Nowadays, it is standard to use Feshbach resonance at the BEC-BCS crossover to realize a BCS Fermi superfluid. Recent experiments have already demonstrated the coexistence of Bose and Fermi superfluids in several realizable systems, ${}^6\text{Li}$ - ${}^7\text{Li}$ [62], ${}^6\text{Li}$ - ${}^{41}\text{K}$ [63], and ${}^6\text{Li}$ - ${}^{174}\text{Yb}$ [64] mixtures, where the heavy species can serve as the impurity at will. The combinations ${}^6\text{Li}$ - ${}^{133}\text{Cs}$ [65], ${}^6\text{Li}$ - ${}^{168}\text{Er}$ [66], and ${}^6\text{Li}$ - ${}^{168}\text{Er}$ [66] are also promising candidates, where the interspecies Feshbach resonances have been characterized.

The rest of this paper is organized as follows. In the following section, we establish our general formalism and show how to extend the exact FDA approach to the case of a BCS superfluid as a background system. Section III is devoted to presenting our numerical results, and Sec. IV is given to the discussion of possible experimental realizations. Finally, we conclude our paper by discussing the physics and proposing applications in Sec. V.

II. FORMALISM

A. Heavy impurity in a BCS superfluid

Our system consists of a static impurity atom, that either is localized by a deep optical lattice or has infinitely heavy mass, and a two-component Fermi superfluid with equal mass $m_\uparrow = m_\downarrow = m$. We assume the impurity can be in either a noninteracting or an interacting hyperfine state with the background fermions, where the many-body Hamiltonian is given by \hat{H}_i and \hat{H}_f , correspondingly. The energy difference of these two hyperfine states only leads to trivial effects and is neglected in this work. The interaction between unlike atoms in the two-component Fermi gas can be tuned by a broad Feshbach resonance, and characterized by the s -wave scattering length a . At low temperature T , these strongly interacting fermions undergo a crossover from a BEC to a BCS superfluid, which can be described by the celebrated BCS theory at a mean-field level and is briefly reviewed here and in Appendix A.

Using the units $\hbar = 1$ hereafter, the BCS Hamiltonian is given by

$$\hat{\mathcal{H}}_i = K_0 + \sum_{\mathbf{k}} \hat{\psi}_{\mathbf{k}}^\dagger \underline{h}_i(\mathbf{k}) \hat{\psi}_{\mathbf{k}}, \quad (1)$$

where $\hat{\psi}_{\mathbf{k}}^\dagger \equiv (c_{\mathbf{k}\uparrow}^\dagger, c_{-\mathbf{k}\downarrow})$ is the Nambu spinor representation with $c_{\mathbf{k}\sigma}^\dagger$ ($c_{\mathbf{k}\sigma}$) being the creation (annihilation) operator for a σ -component fermion with momentum \mathbf{k} . Here, $K_0 \equiv -\mathcal{V}\Delta^2/g + \sum_{\mathbf{k}}(\epsilon_{\mathbf{k}} - \mu)$ with \mathcal{V} denoting the system volume and Δ being the pairing gap parameter. $\epsilon_{\mathbf{k}} \equiv \hbar^2 k^2/2m$ is the single-particle dispersion relation and μ is the chemical potential. We assume the populations of the two components are the same and fixed by μ via the number equation Eq. (A1) [67]. The bare coupling constant g should be renormalized by the s -wave scattering length a between the two components via

$$g^{-1} = \frac{m}{4\pi a} - \sum_{\mathbf{k}}^{\Lambda} \frac{1}{2\epsilon_{\mathbf{k}}}, \quad (2)$$

where Λ is an ultraviolet cutoff. $\underline{h}_i(\mathbf{k})$ can be regarded as a single-particle Hamiltonian \hat{h}_i in momentum space and has a matrix form:

$$\underline{h}_i(\mathbf{k}) = \begin{bmatrix} \xi_{\mathbf{k}} & \Delta \\ \Delta & -\xi_{\mathbf{k}} \end{bmatrix}, \quad (3)$$

where $\xi_{\mathbf{k}} \equiv \epsilon_{\mathbf{k}} - \mu$. For a given scattering length a and temperature T , Δ and μ are determined by a set of the mean-field number and gap equations (see Appendix A).

When the static impurity is in the interacting hyperfine state, the many-particle Hamiltonian is given by

$$\hat{\mathcal{H}}_f = \hat{H}_i + \hat{V} \equiv \hat{H}_i + \sum_{\sigma, \mathbf{k}, \mathbf{q}} \tilde{V}_\sigma(\mathbf{k} - \mathbf{q}) c_{\mathbf{k}\sigma}^\dagger c_{\mathbf{q}\sigma}, \quad (4)$$

where $\tilde{V}_\sigma(\mathbf{k})$ is Fourier transformation of $V_\sigma(\mathbf{r})$, the potential between impurity and σ -component fermion. For a reason which will become clear soon, we would like to express \hat{H}_i and \hat{H}_f in a bilinear form. Defining $\hat{\psi}_{\mathbf{k}}^\dagger = (c_{\mathbf{k}\uparrow}^\dagger, c_{-\mathbf{k}\downarrow}) \equiv (c_{\mathbf{k}}^\dagger, h_{\mathbf{k}}^\dagger)$ and rewriting \hat{V} as

$$\hat{V} = \sum_{\mathbf{k}\mathbf{q}} [\tilde{V}_\uparrow(\mathbf{k} - \mathbf{q}) c_{\mathbf{k}}^\dagger c_{\mathbf{q}} - \tilde{V}_\downarrow(\mathbf{q} - \mathbf{k}) h_{\mathbf{k}}^\dagger h_{\mathbf{q}}] + \sum_{\mathbf{k}} \tilde{V}_\downarrow(0), \quad (5)$$

make the bilinear form apparent. We can write the bilinear form of $\hat{\mathcal{H}}_f$ explicitly,

$$\hat{\mathcal{H}}_f = K_0 + \omega_0 + \sum_{\mathbf{k}\mathbf{q}} \hat{\psi}_{\mathbf{k}}^\dagger \underline{h}_f(\mathbf{k}, \mathbf{q}) \hat{\psi}_{\mathbf{q}}, \quad (6)$$

where $\omega_0 = \sum_{\mathbf{k}} \tilde{V}_\downarrow(0)$ and

$$\underline{h}_f(\mathbf{k}, \mathbf{q}) = \underline{h}_i(\mathbf{k}) \delta_{\mathbf{k}\mathbf{q}} + \begin{bmatrix} \tilde{V}_\uparrow(\mathbf{k} - \mathbf{q}) & 0 \\ 0 & -\tilde{V}_\downarrow(\mathbf{q} - \mathbf{k}) \end{bmatrix} \quad (7)$$

can be regarded as a single-particle Hamiltonian \hat{h}_f in momentum space and in a matrix form. We can see that, \hat{h}_i and \hat{h}_f are the single-particle representative of $\hat{\mathcal{H}}_i$ and $\hat{\mathcal{H}}_f$ up to some constants, respectively.

It is worth noting that, in the many-body Hamiltonian $\hat{\mathcal{H}}_f$ we have assumed that the pairing order parameter Δ remains unchanged by introducing the interaction potential $V_\sigma(\mathbf{r})$. For a nonmagnetic potential ($V_\uparrow = V_\downarrow$) that respects time-reversal symmetry, this is a reasonable assumption, according to Anderson's theorem [1]. For a magnetic potential ($V_\uparrow \neq V_\downarrow$), the local pairing gap near the impurity will be affected, as

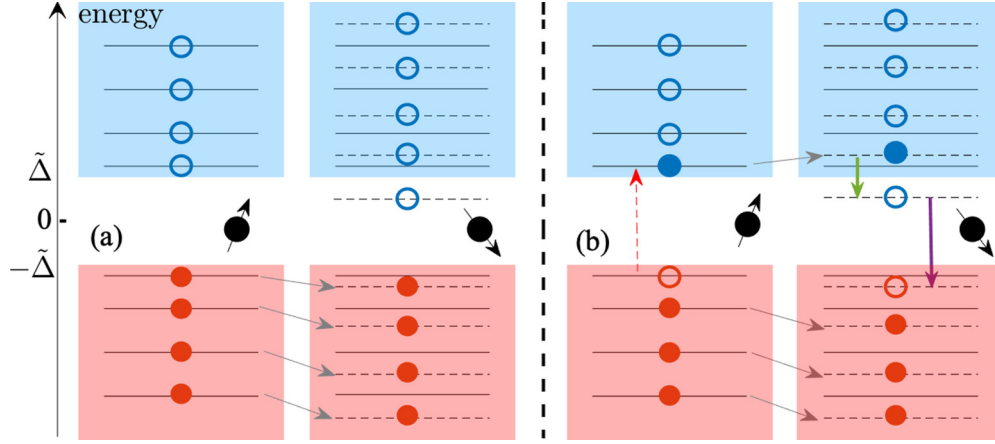


FIG. 1. A sketch of the occupation and structure of the single-particle spectrum of a two-component superfluid Fermi gas at (a) zero temperature and (b) finite temperature. The big black sphere represents the impurity in noninteracting (black arrow up) or interacting (black arrow down) hyperfine state. These spectra always have two-branch structures separated by an energy gap of $2\bar{\Delta}$, where the red and blue rectangles represent the negative and blue branches, respectively. However, the individual energy level with or without impurity interaction have shifts as indicated by the black solid and dashed lines, correspondingly. There also exists an in-gap YSR bound state if the impurity interaction is magnetic ($a_{\uparrow} \neq a_{\downarrow}$).

indicated by the presence of the YSR bound state. We will follow the typical non-self-consistent treatment of the magnetic potential in condensed matter physics [1,57] and assume a constant pairing gap as the first approximation for simplicity. We leave a more rigorous self-consistent calculation of a pairing gap to future studies.

B. Functional determinant approach

We are interested in a situation where the impurity is driven from a noninteracting hyperfine state to an interacting hyperfine state at $t = 0$, as sketched in Fig. 1. The most basic quantity to describe the response to this process is the time-overlapping function

$$S(t) = \langle e^{i\hat{\mathcal{H}}_i t} e^{-i\hat{\mathcal{H}}_f t} \rangle \equiv \text{Tr}[e^{i\hat{\mathcal{H}}_i t} e^{-i\hat{\mathcal{H}}_f t} \hat{\rho}_0], \quad (8)$$

where $\hat{\rho}_0$ is the initial thermal density matrix, and \hat{H}_i and \hat{H}_f are the many-body Hamiltonian with the impurity in noninteracting and interacting hyperfine state, respectively. The response in frequency domain can be obtained via a Fourier transformation

$$A(\omega) = \frac{1}{\pi} \text{Re} \int_0^{\infty} e^{i\omega t} S(t) dt, \quad (9)$$

which is also called spectral function.

We review our main theoretical tool, FDA, and show how to extend this method to the case of an ultracold BCS superfluid as the background medium. An exact calculation of Eq. (8) is usually not accessible due to the exponentially growing complexity of the many-body Hamiltonian with respect to particle number N . However, one can prove that Eq. (8) can reduce to a determinant in a single-particle Hilbert space that grows only linearly to N , if \hat{H}_i and \hat{H}_f are both fermionic [45,68,69], bilinear many-body operators, such as Eq. (1) and Eq. (6) shown in the previous section. In that case, we have

$$S(t) = e^{-i\omega_0 t} \det[1 - \hat{n} + e^{i\hat{h}_i t} e^{-i\hat{h}_f t} \hat{n}], \quad (10)$$

where \hat{n} is the occupation number operator (see Appendix B for details).

It would be more convenient to carry out numerical calculations in the coordinate space in a finite system confined in a sphere of radius R . We then take the system size towards infinity, while keeping the density constant, until numerical results are converged. The bilinear form of the many-body Hamiltonians in coordinate space are given by

$$\hat{\mathcal{H}}_i = K_0 + \int d\mathbf{r} \hat{\phi}^\dagger(\mathbf{r}) \underline{h}_i(\mathbf{r}) \hat{\phi}(\mathbf{r}), \quad (11)$$

$$\hat{\mathcal{H}}_f = K_0 + \omega_0 + \int d\mathbf{r} \hat{\phi}^\dagger(\mathbf{r}) \underline{h}_f(\mathbf{r}) \hat{\phi}(\mathbf{r}), \quad (12)$$

with $K_0 = -\mathcal{V}\Delta^2/g + \sum_{\mathbf{k}} (\epsilon_{\mathbf{k}} - \mu)$ being an unimportant constant that cancels out in Eq. (10). Here, $\hat{\phi}^\dagger(\mathbf{r}) = [c_{\uparrow}^\dagger(\mathbf{r}), c_{\downarrow}^\dagger(\mathbf{r})] \equiv [c^\dagger(\mathbf{r}), h^\dagger(\mathbf{r})]$ are creation operators in the coordinate space. Since higher partial wave interaction is negligible at low temperature, we focus on the s -wave channel. We also assume $V_\sigma(\mathbf{r}) = V_\sigma(r)$ is spherically symmetric and short-range. The single-particle representative of Hamiltonians in coordinate space, therefore, are given by

$$\begin{aligned} \underline{h}_f(r) &= \underline{h}_i(r) + \begin{pmatrix} V_{\uparrow}(r) & 0 \\ 0 & -V_{\downarrow}(r) \end{pmatrix} \\ &\equiv \begin{pmatrix} -\frac{1}{2m} \frac{d^2}{dr^2} + V_{\uparrow}(r) - \mu & \Delta \\ \Delta & \frac{1}{2m} \frac{d^2}{dr^2} - V_{\downarrow}(r) + \mu \end{pmatrix}. \end{aligned} \quad (13)$$

In our numerical calculation, we choose a soft-core van-der-Waals potential

$$V_\sigma(r) = -\frac{C_6}{r^6} \exp\left[-\frac{r_\sigma^6}{r^6}\right], \quad (14)$$

where C_6 is the dispersion coefficient describing the long-range behavior of the impurity-fermion interaction and determines the van-der-Waals length $l_{\text{vdW}} = (2mC_6)^{1/4}/2$. The short-range parameter r_σ are tuned to give the desired

energy-dependent scattering length

$$a_\sigma(E_F) = -\frac{\tan \eta_\sigma(k_F)}{k_F}, \quad (15)$$

where $\eta_\sigma(k_F)$ is the s -wave scattering length between the impurity and σ -component fermions at the Fermi energy $E_F = k_F^2/2m$. We find our calculations are insensitive to other details of $V_\sigma(r)$ (such as the value of l_{vdW} and the number of short-range bound states the potential supported) as long as $k_F l_{\text{vdW}} \ll 1$. Therefore we denote $a_\sigma(E_F) \equiv a_\sigma$ hereafter for the simplicity of notation. In the calculations here, we choose $k_F l_{\text{vdW}} = 0.01$ unless specify otherwise. To calculate Eq. (10), we need to find the eigenpairs $E_\nu, \phi_\nu \equiv [\phi_{\nu,\uparrow}(r), \phi_{\nu,\downarrow}(r)]$ for $h_i(r)$ and $\tilde{E}_\nu, \tilde{\phi}_\nu$ for $h_f(r)$, and express the occupation operator \hat{n} as a diagonal matrix with elements

$$n_{\nu\nu} = f(E_\nu) = \frac{1}{e^{E_\nu/k_B T} + 1}. \quad (16)$$

We also need to take care of ω_0 if $V_\downarrow \neq 0$. Noticing that the original definition $\omega_0 = \sum_{\mathbf{k}} \tilde{V}_\downarrow(0) = \sum_{\mathbf{k}} \int d\mathbf{r} \langle \mathbf{k} | \mathbf{r} \rangle V(\mathbf{r}) \langle \mathbf{r} | \mathbf{k} \rangle$ is equivalent to taking the trace of the matrix representative of \tilde{V}_\downarrow in momentum state basis (see Appendix C). Therefore ω_0 can also be obtained via tracing \tilde{V}_\downarrow in an arbitrary complete orthogonal set of basis, i.e., $\omega_0 = \text{Tr} \tilde{V}_\downarrow$. The details on the discretization basis set and other technical issues of numerical calculations are presented in Appendix C.

We give a few further remarks on some possible extensions of our methods. As already noticed in Ref. [7], generalization of FDA to other geometries and confinement can be easily implemented to the single-particle Hamiltonian. Our single-channel soft-core van der Waals potential have been proved to mimic the interatomic interaction near broad Feshbach resonances very well [70] and can be replaced by multichannel interactions to describe closed-channel dominated Feshbach resonances.

III. RESULTS

A. Single-particle spectrum

It is illustrative to first see the structure of a single-particle spectrum, as sketched in Fig. 1. When the impurity interaction is absent, diagonalizing $h_i(r)$ gives the well-known BCS dispersion relation

$$E_\nu = \pm \mathcal{E}_{k_\nu} = \pm \sqrt{\xi_{k_\nu}^2 + \Delta^2}, \quad (17)$$

where $k_\nu R = n_\nu \pi$ with integer n_ν . The positive and negative branches of the spectrum are separated by an energy gap

$$2\tilde{\Delta} = \begin{cases} 2\Delta & \mu \geq 0 \\ 2\sqrt{\Delta^2 + \mu^2} & \mu < 0 \end{cases}, \quad (18)$$

which represents the minimum energy required to break a Cooper pair into a particle-hole excitation. At zero temperature, the many-body ground state can be regarded as a fully filled Fermi sea of the lower branch, and a completely empty Fermi sea of the upper branch. [Notice that the E_ν are measured with respect to chemical potential μ , which leads to the occupation $f(E_\nu) = 1/(e^{-E_\nu/k_B T} + 1)$].

In the presence of impurity interaction, our numerical calculations show that \tilde{E}_ν still consists of two branches separated

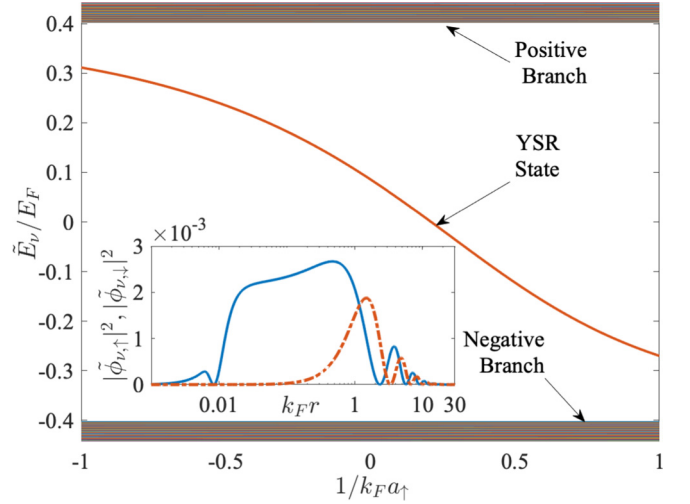


FIG. 2. Single-particle spectrum of a Fermi superfluid with a magnetic impurity ($a_\downarrow = 0$) as a function of $1/(k_F a_\uparrow)$. The scattering length between the two-component fermions is $k_F a = -2$, which gives rise to $\mu \simeq 0.85E_F$ and $\Delta \simeq 0.40E_F$ at zero temperature. The solid red curve in the middle shows the YSR bound state energy. The inset shows the corresponding YSR wave functions $\tilde{\phi}_{\nu,\uparrow}$ (blue solid curve) and $\tilde{\phi}_{\nu,\downarrow}$ (red dash-dotted curve) at $k_F a_\uparrow = -2$.

by $2\tilde{\Delta}$, with each individual energy level shifted as shown in Fig. 1. Moreover, when the impurity scattering is magnetic ($a_\uparrow \neq a_\downarrow$), a subgap YSR bound state exists. Figure 2 shows the YSR bound state energy as a function of $1/(k_F a_\uparrow)$ for the case $k_F a = -2$ and $k_F a_\downarrow = 0$ at zero temperature. The decreasing bound state energy with increasing $1/(k_F a_\uparrow)$ can be qualitatively understood from the analytic expression

$$E_{\text{YSR}} \simeq \Delta \cos[\eta_\uparrow(E_F) - \eta_\downarrow(E_F)], \quad (19)$$

which holds in the weak-coupling limit ($a \rightarrow 0^-$) [59]. Here, $\eta_\uparrow(E_F)$ and $\eta_\downarrow(E_F) = 0$ are the impurity scattering phase shifts of the potentials $V_\uparrow(r)$ and $V_\downarrow(r)$ at Fermi energy E_F . The inset of Fig. 2 shows the YSR wave function at $k_F a_\uparrow = -2$, where one can see that the YSR bound state has a relatively large size (about $30k_F^{-1}$ in this case) and shows an oscillation behavior at large distances.

We give some further remarks here on the two-body bound states supported solely by the short-range potential $V_\sigma(r)$, when the other component of fermions are absent. In general, there are multiple such bound states, and almost all of them are deeply bound with large binding energy $E_b \gg \Delta$ and highly localized to the impurity. As a result, the overlapping between these deeply bound states and BCS scattering waves are vanishingly small. Therefore these deeply bound states are almost unaffected by the presence of the other component and give negligible effects on the response functions. The only exception is the shallowest bound state with $a_\sigma > 0$. This shallow bound state can strongly couple to the scattering states of the other component, and hence can no longer be distinguished from the eigenstates $\tilde{\phi}_\nu$.

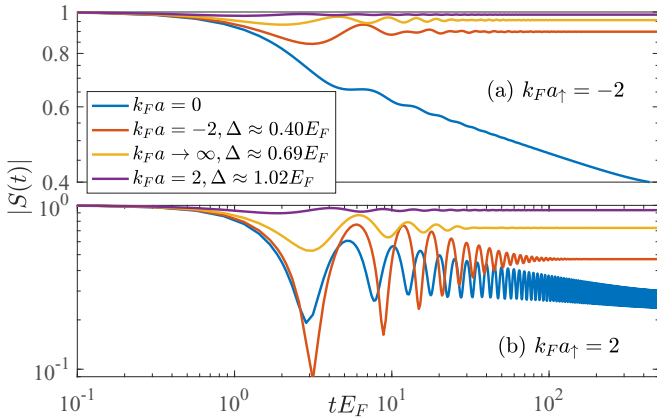


FIG. 3. Zero-temperature Ramsey responses $|S(t)|$ for a magnetic impurity ($a_\downarrow = 0$) scattering with (a) attractive scattering lengths $a_\uparrow < 0$ and (b) repulsive scattering lengths $a_\uparrow > 0$ are shown for different values of the scattering length a between the two-component fermions; see legend.

B. Magnetic impurity

We first focus on the simplest case, where the impurity only interacts with the spin-up component, i.e., $a_\downarrow = 0$.

When $\Delta = 0$ and $a_\downarrow = 0$, our system reduces back to an ideal Fermi gas (consisting of spin-up fermions) [3,7], and the asymptotic behavior of the Ramsey response at $t \rightarrow \infty$ is given by

$$S(t) \simeq C e^{-i\Delta E t/\hbar} \left(\frac{1}{iE_F t/\hbar + 0^+} \right)^\alpha + C_b e^{-i(\Delta E - E_F + E_b)t/\hbar} \left(\frac{1}{iE_F t/\hbar + 0^+} \right)^{\alpha_b}, \quad (20)$$

where C and C_b are both numerical constants independent with respect to $k_F a$ and $C_b = 0$ for $a_\uparrow < 0$. Here,

$$\alpha = \eta_\uparrow(E_F)^2/\pi^2 \quad (21)$$

and

$$\alpha_b = [1 + \eta_\uparrow(E_F)/\pi]^2 \quad (22)$$

are determined by the scattering phase shifts $\eta_\uparrow(E_F)$ at Fermi energy. E_b is the binding energy of the shallowest bound state consisting of the impurity and a spin-up fermion for $a_\uparrow > 0$ and $\Delta = 0$. Furthermore, the change in energy is given by

$$\Delta E = \sum_{E_\nu < 0} (E_\nu - \tilde{E}_\nu), \quad (23)$$

where deeply bound states are excluded from \tilde{E}_ν . Notice that the power-law decaying behavior of $|S(t)|$ at $\Delta = 0$ is evident in Fig. 3 (see the blue lines).

In sharp contrast, for cases with nonzero pairing gap, the asymptotic behavior in the long-time limit shows that $|S(t \rightarrow \infty)| \propto t^0$ approach to some constants. These asymptotic constants are larger for larger Δ . Further details can be obtained by an asymptotic form that fits our numerical calculations perfectly well, as reported in Fig. 4,

$$S(t) \simeq D_a e^{-iE_a t} + D_r e^{-iE_r t}, \quad (24)$$

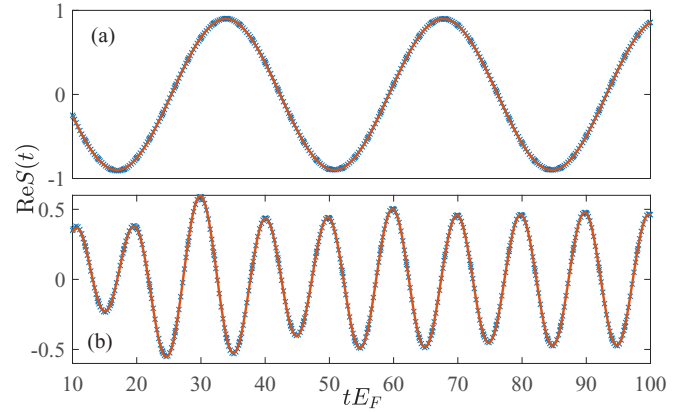


FIG. 4. Fitting asymptotic behavior of $\text{Re}S(t)$ at zero temperature for a magnetic impurity ($a_\downarrow = 0$) that only interacts with spin-up component of the Fermi superfluid with $k_F a = -2$ for (a) $k_F a_\uparrow = -2$ and (b) $k_F a_\downarrow = 2$. The cross symbols are the numerical results, and the solid curves correspond to the fitting formula Eq. (24).

where $D_r = 0$ for $a_\uparrow < 0$. We obtain D_a , D_r , E_a , and E_r from fitting, and find that $E_r = \text{Re}E_r + i\text{Im}E_r$ is in general complex. In contrast, $E_a = \sum_{E_\nu < 0} (E_\nu - \tilde{E}_\nu)$ (where \tilde{E}_ν excludes the two-body deeply bound states) is purely real, and can be explained as a renormalization of the filled Fermi sea, as indicated by the grey arrows in Fig. 1(a).

The long-time asymptotic behavior of $S(t)$ manifests itself as some characterized lineshape in the spectral function

$$A(\omega) \propto \begin{cases} Z_a \delta(\omega - E_a) & \omega \approx E_a \\ Z_r \frac{|\text{Im}E_r|/\pi}{(\omega - \text{Re}E_r)^2 + (\text{Im}E_r)^2} & \omega \approx \text{Re}E_r \end{cases}, \quad (25)$$

i.e., a δ function around E_a and a Lorentzian around $\text{Re}E_r$. The existence of δ -function peak unambiguously confirms the existence of a well-defined quasiparticle—the attractive polaron with energy E_a . The Lorentzian, on the other hand, can be recognized as a repulsive polaron with finite width and hence finite lifetime. Here, $Z_a = |D_a|$ and $Z_r = |D_r|$ are the residue of attractive and repulsive polarons, correspondingly. Numerically, we find that $Z_a \propto (\Delta/E_F)^{\alpha_a}$ and $Z_r \propto (\Delta/E_F)^{\alpha_r}$ at small Δ as shown in the insets of Figs. 5(a) and 5(b). As a result, Eq. (24) have the same form as Eq. (20), the analytic expression of $S(t)$ for a noninteracting Fermi gas medium, if we replace the low-energy cutoff $1/t \rightarrow \Delta$. However, the power-law coefficients α_a and α_r are only close to but not exactly the same as the analytical expressions of α and α_b . In the inset of Fig. 5(a), our numerical fitting gives $\alpha_a \approx 0.136$, comparing with $\alpha \approx 0.124$ for ideal Fermi gases. In the inset of Fig. 5(b), $\alpha_r \approx 0.083$ and $\alpha_a \approx 0.452$, in compare with $\alpha \approx 0.124$ and $\alpha_b \approx 0.419$. These small differences are probably due to the modification of scattering phase shifts in the presence of Δ .

Next, we study the full zero-temperature polaron spectrum across the BEC-BCS crossover and show them in Fig. 5. Numerically, to obtain $A(\omega)$ accurately requires a Fourier transformation that involves an integration of $S(t)$ from $t = 0$ to $t \rightarrow \infty$. We follow the procedures adopted from Ref. [7]: we numerically integrate $S(t)$ up to some large cutoff time $t^* \sim 500/E_F$ and carry-out the integration analytically with the fitting formula Eq. (24) for $t > t^*$.

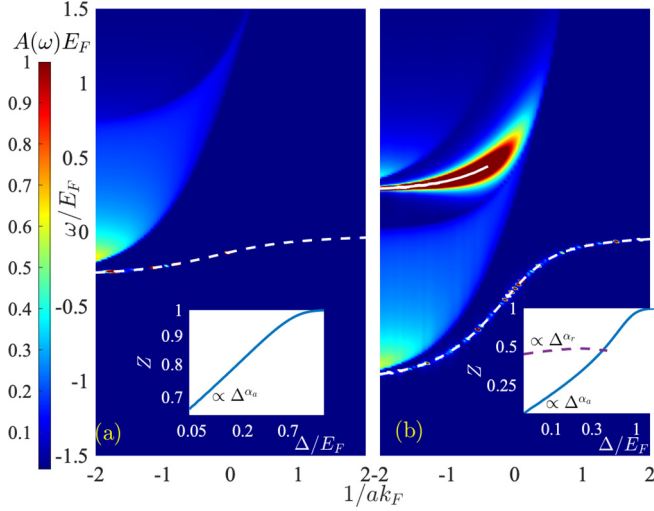


FIG. 5. Zero-temperature polaron spectra with $a_\downarrow = 0$ for (a) $k_F a_\uparrow = -2$ and (b) 2 as a function of $1/(k_F a)$ at the BEC-BCS crossover. The white dashed and solid curves corresponds to the attractive (E_a) and repulsive (E_r) polaron energy, respectively. The insets shows the residues of the polarons. The blue solid curves and the purple dashed curves show the residue of attractive polaron Z_a and repulsive polaron Z_r , respectively, as a function of Δ , which show power-law behaviors at small Δ .

Figure 5(a) shows the case $k_F a_\uparrow = -2 > 0$, where the white dashed curve indicates the attractive polaron δ -function peak. This attractive polaron separates from a molecule-hole continuum by a region of anomalously low spectral weight, namely the “dark continuum” (also shown in the inset of Fig. 6). The existence of dark continuum has been previously observed in spectra of other polaron systems. However, most of these studies apply various approximations, and only recently a diagrammatic Monte Carlo study proves the dark continuum is indeed physical [35]. Here, our FDA calculation of the heavy crossover polaron spectrum gives an exact proof of the dark continuum. In addition, we can see that the dark continuum regime becomes smaller towards the deep BCS

side of the Feshbach resonance for the background Fermi superfluid. We expect that the dark continuum vanishes in the $\Delta \rightarrow 0$ limit, and the attractive polaron will merge into the molecule-hole continuum, forming a power-law singularity seen in the spectrum of heavy impurity in an ideal Fermi gas [7].

The white solid curve in Fig. 5(b) shows the repulsive polaron energy. We can observe that the repulsive polaron width become larger from the BCS side towards the unitary limit. Near the unitary limit, the repulsive polaron residue Z_r also deviates from the power law-dependence and starts decreasing as shown in the inset of Fig. 5(b). Towards the BEC side, both the repulsive polaron and the molecule-hole continuum are vanishing, which can also be inferred from the behavior $Z_a \rightarrow 1$ on the deep BEC side.

We also study the finite-temperature spectrum at $k_F a = -2$ as shown in Fig. 6. Figures 6(a) and 6(b) show the spectrum at $k_F a_\uparrow = -2$ and $k_F a_\uparrow = 2$, respectively. As temperature increases, we observe the expected thermal broadening and slightly shifts of the spectral peaks since Δ reduces at finite temperature. Interestingly, we also observe some additional features. An onset of spectral weight enhancement arises sharply at the energy

$$E_{\text{YSR}}^{(-)} = E_a - (\Delta - E_{\text{YSR}}), \quad (26)$$

below the attractive polaron. We explain this feature as an additional decay from the upper branch state to the subgap YSR state illustrated by the green arrow in Fig. 1(b). There is also another feature that associates with the repulsive polaron shows up for the $k_F a_\uparrow = 2$ case at energy

$$E_{\text{YSR}}^{(+)} = \text{Re}(E_r) - (E_{\text{YSR}} + \Delta), \quad (27)$$

which implies that this feature is related to the decay from the YSR state back to the lower branch as illustrated by the purple arrow in Fig. 1(b). These two decay processes are only allowed if the upper branch has thermal occupations initially, which explain why such features only show up at finite temperature. These features can be better depicted in

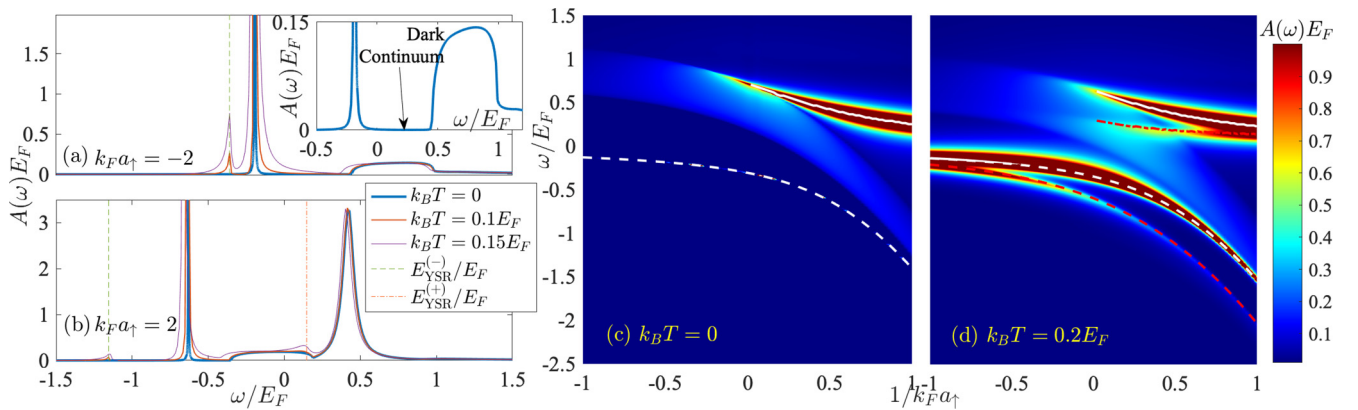


FIG. 6. Polaron spectra with $k_F a = -2$ and $a_\downarrow = 0$ at different temperature (see legend) with (a) $k_F a_\uparrow = -2$ and (b) 2, with the green dashed and red dash-dotted vertical lines indicates the YSR features $E_{\text{YSR}}^{(-)}$ and $E_{\text{YSR}}^{(+)}$, respectively. A zoom-in of the dark spectrum at zero temperature is shown in the inset. A small artificial width is added to the δ -function peak at zero temperature for visibility. The full spectra as a function of $1/(k_F a_\uparrow)$ are shown in (c) at zero temperature and (d) $k_B T = 0.2$. The white dashed and solid curves shows the attractive and repulsive polaron energies, respectively. The red dashed and dash-dotted in (d) corresponds to $E_{\text{YSR}}^{(-)}$ and $E_{\text{YSR}}^{(+)}$, respectively.

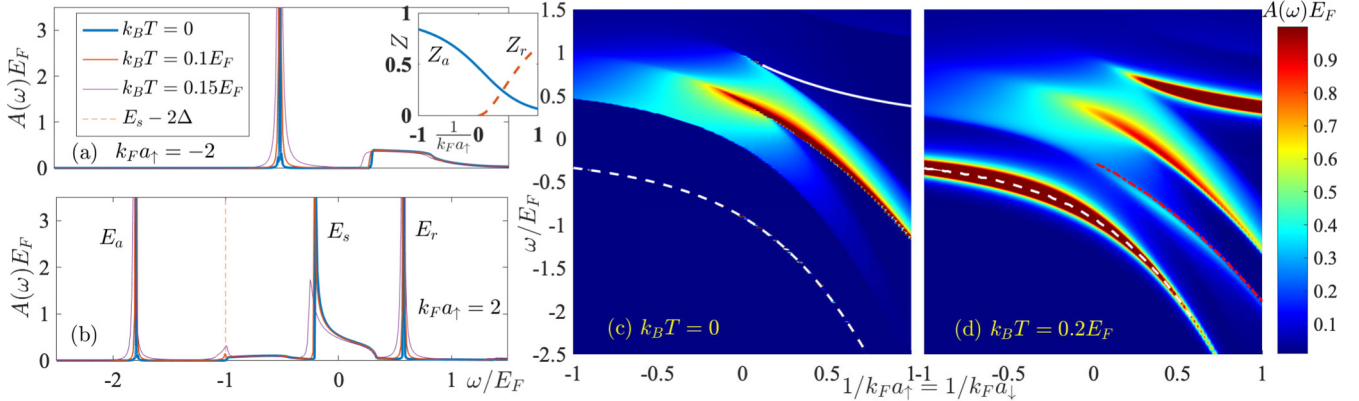


FIG. 7. Polaron spectrum of heavy nonmagnetic impurity ($a_\uparrow = a_\downarrow$) in a BCS superfluid with $k_F a = -2$ at different temperature (see legend). The impurity scattering length is (a) $k_F a = -2$ and (b) 2. The red dashed vertical line shows a feature at $E_s - 2\Delta$ associated with the singularity at E_s . The inset shows the residue as a function of $1/(k_F a_\uparrow)$. The full spectrum as a function of $1/(k_F a_\uparrow)$ are shown in (c) and (d) for zero and finite temperature, respectively. The white dashed and solid curves shows attractive and repulsive polaron energy, and the red dash-dotted curve shows the finite temperature feature.

the comparison of the full spectra as a function of $1/(k_F a_\uparrow)$ at zero and finite temperature in Figs. 1(c) and 1(d), respectively.

C. Nonmagnetic impurity

In this section, we study the case of nonmagnetic impurity scattering $a_\uparrow = a_\downarrow$, where the YSR state merges into the upper branch states as a result of Eq. (19) and ceases to exist.

As expected, Fig. 7(a) shows no YSR features at $k_F a = -2$ and is quite simple. In contrast, the polaron spectra on the positive side $k_F a_\uparrow = 2$ are much more complex as depicted in Fig. 7(b). Interestingly, the repulsive polaron at zero temperature is also characterized by a δ function with infinite lifetime. In addition, another singularity shows up at E_s . We speculate the new long-lived repulsive polaron is related to undamped density excitations (i.e., the gapless Goldstone mode of the Fermi superfluid) excited by the nonmagnetic impurity potential. As the coupling to the gapless Goldstone mode does not cost energy, the OC mechanism may lead to a power-law singularity, which is the reminiscent of the damped repulsive polaron in the case of magnetic impurity scattering. With this understanding in mind, we have checked that the asymptotic $t \rightarrow \infty$ behavior fits the formula

$$S(t) \approx D_a e^{-iE_a t} + D_r e^{-iE_r t} + D_s e^{-iE_s t} \left(\frac{1}{iE_F t} \right)^{\alpha_s} \quad (28)$$

very well, as shown in Fig. 8(a). Our numerical fitting confirms E_a , E_r , and E_s are all purely real. We also find that the power-law component of the singularity $\alpha_s \approx 0.5$, which seems to be a constant insensitive to a_\uparrow , a_\downarrow , and a . The residue $Z_a = |D_a|$ and $Z_r = |D_r|$ as a function of impurity interaction $1/(k_F a_\uparrow)$ are shown in the inset of Fig. 7(a), which shows that the attractive polaron residue decreases and repulsive polaron becomes dominated on the positive side of impurity scattering length $a_\uparrow > 0$. The dependence of Z_a and Z_r on Δ is reported in Fig. 8(b). Similar to the magnetic impurity case, we observe the power-law dependences $Z_a \propto (\Delta/E_F)^{\alpha_a}$ and $Z_r \propto (\Delta/E_F)^{\alpha_r}$ at small Δ , and $Z_a \rightarrow 1$ and $Z_r \rightarrow 0$ on the deep BEC side $\Delta \rightarrow \infty$.

Figures 7(c) and 7(d) show the comparison between zero and finite temperature polaron spectrum as a function of $1/(k_F a_\uparrow)$. We can observe a finite temperature feature appears at $E_s - 2\Delta$, as shown in red dash-dotted curve in Fig. 7(d) [as indicated by the dashed vertical line in Fig. 7(b) at $k_F a_\uparrow = 2$]. This feature is the reminiscent of the structure at $E_{\text{YSR}}^{(+)}$ in the case of magnetic impurity scattering [see Eq. (27)], if we recall the replacement $\text{Re}E_r \rightarrow E_s$ and $E_{\text{YSR}} = \Delta$ as a result of the dissolution of the YSR state into the upper branch single-particle states.

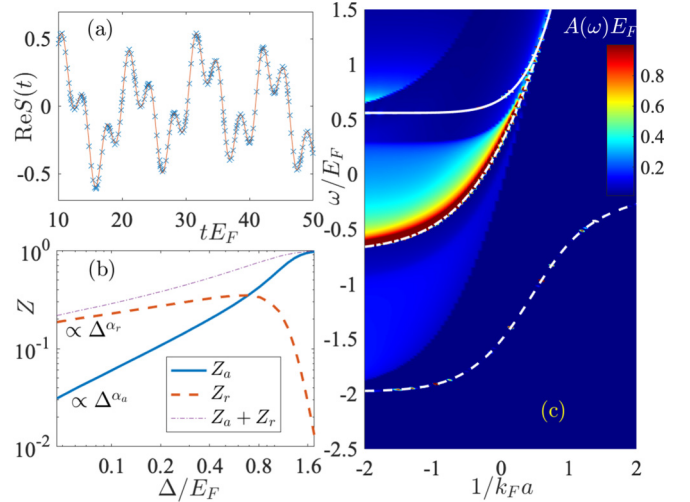


FIG. 8. (a) $\text{Re}S(t)$ as a function of t , the cross symbol shows the numerical result, and the solid line is the fitting formula Eq. (28). (b) The polaron residue as a function of Δ . The blue solid, red dashed and purple dash-dotted curves correspond to Z_a , Z_r , and $Z_a + Z_r$, respectively. The power-law exponents $\alpha_a \approx 0.85$ and $\alpha_r \approx 0.25$. (c) Polaron spectrum of heavy nonmagnetic impurity ($k_F a_\uparrow = k_F a_\downarrow = 2$) at zero temperature as a function of $1/(k_F a)$ at the BEC-BCS crossover. The white solid, dash and dash-dotted curve corresponds to the repulsive polaron, attractive polaron and the singularity energy, respectively.

Finally, we present the spectrum across the BEC-BCS crossover as a function of $1/(k_F a)$ in Fig. 8(c). Towards the BEC side, we observe that the spectral weight of the singularity decreases [which can be implied by the increase of $Z_a + Z_r$ shown in Fig. 8(b)]. Eventually, the singularity and the repulsive polaron merges at around $1/(k_F a) \simeq 0.5$, which coincides where the chemical potential μ is changing from positive to negative.

IV. EXPERIMENTAL REALIZATION

Our predictions could be readily examined in cold-atom experiments. Indeed, several quantum mixtures consisting of a Fermi superfluid and a Bose condensate have already been demonstrated, including ${}^6\text{Li}$ - ${}^7\text{Li}$ [62], ${}^6\text{Li}$ - ${}^{41}\text{K}$ [63], and ${}^6\text{Li}$ - ${}^{174}\text{Yb}$ [64] mixtures. Quantum mixtures such as ${}^6\text{Li}$ - ${}^{133}\text{Cs}$ [65], ${}^6\text{Li}$ - ${}^{168}\text{Er}$ [66], and ${}^6\text{Li}$ - ${}^{168}\text{Er}$ [66] should also be available soon, since the interspecies Feshbach resonances have been characterized recently. In these mixtures, polaron physics can be explored by reducing the concentration of the bosonic component. For ${}^6\text{Li}$ - ${}^{174}\text{Yb}$, ${}^6\text{Li}$ - ${}^{133}\text{Cs}$, and ${}^6\text{Li}$ - Er systems, the minority bosonic species have different polarizability, which allows imposing a deep optical lattice to localize the impurity without affecting much the itinerant fermions. Even without the optical lattice, our calculations still give quantitatively accurate predictions due to the extremely large mass ratio. The response functions predicted here can be measured via established methods: $S(t)$ can be accessed via an interferometric Ramsey scheme; $A(\omega)$ can be obtained in rf-spectroscopy.

As a concrete example, let us focus on the ${}^6\text{Li}$ - ${}^{133}\text{Cs}$ mixture. Nowadays, a two-component Fermi superfluid of ${}^6\text{Li}$ atoms in the lowest two energy hyperfine states $|1, 2\rangle = |F = 1/2, m_F = \pm 1/2\rangle$ is a typical setup to realize the BEC-BCS crossover in cold-atom laboratories, owing to a broad Feshbach resonance at $B_0 \simeq 832$ G. The Feshbach resonances between ${}^{133}\text{Cs}$ and ${}^6\text{Li}$ have been accurately calibrated in 2013 [65]. Remarkably, in its lowest energy state $|a\rangle = |F = 3, m_F = 3\rangle$ ${}^{133}\text{Cs}$ atoms have a broad Feshbach resonance near B_0 with ${}^6\text{Li}$ atoms in both hyperfine states $|1, 2\rangle$. The resonances locate at $B_{0\uparrow} = 843.4(2)$ G for $|\text{Li} : 1\rangle + |\text{Cs} : a\rangle$ and $B_{0\downarrow} = 889.0(2)$ G for $|\text{Li} : 2\rangle + |\text{Cs} : a\rangle$. The three closely located broad Feshbach resonances mean that we can conveniently tune the magnetic field, to reach three significant scattering lengths a , a_\uparrow and a_\downarrow at the same time. In particular, by sweeping the magnetic field near $B_{0\uparrow} = 843.4(2)$ G, the parameter sets used in Fig. 6 and Fig. 7 can be easily realized.

Since our theoretical treatment assumes the impurity mass is infinitely large, it would be necessary to analyze the finite mass effect. Such effect can be estimated by comparing the recoil energy and superfluid gap Δ , both of which play the role of suppressing multiple particle-hole excitations. From momentum and energy conservation, the recoil momentum of a fermion at fermi momentum k_F on a heavy impurity with mass M is approximately $2mk_F/M$ if $m/M \ll 1$. The recoil energy thus is given by $E_{\text{recoil}} = (2mk_F/M)^2/2m = (4m^2/M^2)E_F$. Therefore the finite mass effect can be neglected if $E_{\text{recoil}} \ll 2\Delta$ or equivalently $m/M \ll \sqrt{\Delta/2E_F}$. For ${}^6\text{Li}$ - ${}^{133}\text{Cs}$, the mass ratio $m/M \approx 0.045$ ensures that our predictions for $\Delta \geq 0.1E_F$ are valid. A more quantitative

investigation can be a comparison with the Chevy ansatz predictions, such as Ref. [55], for large impurity mass systems, which will be explored in future studies. On the other hand, one can also localize the impurity via a strong optical lattice, and essentially eliminate the finite mass effect [3,7].

V. DISCUSSIONS AND APPLICATIONS

The present work shows how to generalize FDA to the system of a heavy impurity immersed in a BCS superfluid. This formalism allows us to construct an exact model to investigate polaron physics, which gives all the universal polaron features, such as attractive and repulsive polaron, dark continuum, and molecule-hole continuum. In our model, the existence of polarons is protected from OC since the superfluid pairing gap suppresses multiple particle-hole excitations, which plays a similar role as the recoil energy of a mobile impurity in conventional Fermi polarons. In addition, we have shown in an accompanying paper [48] that the pairing gap can also protect the polarons from thermal fluctuations, allowing experimental studies at a more accessible temperature $k_B T \sim \Delta$. Our results for the nonmagnetic impurity case also show some surprising results: the existence of a repulsive polaron with an infinite lifetime and an additional singularity. These peculiar characteristics only occur at the perfect balance of the two scattering lengths, where the impurity can only excite gapless density fluctuations. It would be interesting to find an intuitive understanding of the underlying physics in future studies.

Our predictions can also be applied to measure various exciting features of the Fermi superfluid, although the BCS description is only quantitatively reliable on the BCS side, and become only qualitatively reliable near the unitary limit and the BEC side. The BCS description also eliminates the collective bosonic excitation, which might become important in the deep BEC side and induce OC. We will nevertheless neglect such excitations in this first study. In the magnetic impurity case, the polaron spectrum at a finite but low temperature shows sharp features that measure the subgap YSR bound states. In particular, if E_a , $\text{Re}(E_r)$, $E_{\text{YSR}}^{(-)}$ and $E_{\text{YSR}}^{(+)}$ shown in Fig. 6(d) are all measured accurately, Eqs. (26) and (27) give rise to

$$2\Delta = E_a + \text{Re}(E_r) - E_{\text{YSR}}^{(-)} - E_{\text{YSR}}^{(+)}, \quad (29)$$

independent on E_{YSR} . We believe that this relation may only depend on the existence of a pairing gap and an in-gap bound state, and therefore holds independent of the theoretical model used in this work. This allows a highly accurate measurement of the pairing gap Δ at the whole BEC-BCS crossover. In the nonmagnetic impurity case, there is also a finite temperature feature associated with the singularity $E_s - 2\Delta$, which can be applied to measure the pairing gap Δ .

ACKNOWLEDGMENTS

We are grateful to Xing-Can Yao for insightful discussions. This research was supported by the Australian Research Council's (ARC) Discovery Program, Grants No. DE180100592 and No. DP190100815 (J.W.), and Grant No. DP180102018 (X.-J.L.).

APPENDIX A: THE BCS-LEGGETT THEORY OF THE BEC-BCS CROSSOVER

For a given scattering length a and temperature T , Δ , and μ are determined by the mean-field number and gap equations:

$$\sum_{\mathbf{k}} \left[1 - \frac{\xi_{\mathbf{k}}}{E_{\mathbf{k}}} + 2 \frac{\xi_{\mathbf{k}}}{E_{\mathbf{k}}} f(E_{\mathbf{k}}) \right] = n, \quad (\text{A1})$$

$$\frac{m}{4\pi a} + \sum_{\mathbf{k}} \left[\frac{1 - 2f(E_{\mathbf{k}})}{2E_{\mathbf{k}}} - \frac{1}{2\epsilon_{\mathbf{k}}} \right] = 0, \quad (\text{A2})$$

where $f(E_{\mathbf{k}}) = [\exp(-E_{\mathbf{k}}/k_B T) + 1]^{-1}$ is the Fermi-Dirac distribution, with k_B is the Boltzmann constant. Here $E_{\mathbf{k}} = \sqrt{\xi_{\mathbf{k}}^2 + \Delta^2}$ are the eigenvalues of Eq. (3) with the corresponding eigenvector $[u_{\mathbf{k}}, v_{\mathbf{k}}]^T$, where $u_{\mathbf{k}}^2 = [1 + \xi_{\mathbf{k}}/E_{\mathbf{k}}]/2$, $v_{\mathbf{k}}^2 = 1 - u_{\mathbf{k}}^2$, and $2u_{\mathbf{k}}v_{\mathbf{k}} = \Delta/E_{\mathbf{k}}$.

APPENDIX B: DERIVATION OF FDA

Here, we provide details on extending the FDA to the case of an ultracold BCS superfluid as the background medium. Specifically, we aim to prove how Eq. (8) reduces to Eq. (10). Our derivation closely follows the spirit of Ref. [45] on deriving Levitov's formula, which relates certain traces of many-body operators in Fock space to single-particle determinants. Equation (8) of Ref. [45] shows that

$$\text{Tr}[e^{\Gamma(\hat{A})} e^{\Gamma(\hat{B})}] = \det(1 + e^{\hat{A}} e^{\hat{B}}) \quad (\text{B1})$$

for second quantized fermionic operators quadratic in Fock space

$$\Gamma(A) = \sum_{i,j} \langle i | \hat{A} | j \rangle a_i^\dagger a_j, \quad (\text{B2})$$

where \hat{A} is the corresponding single-particle operator and a_i^\dagger and a_i are the creation and annihilation operators for a given one particle state i . The matrix \underline{A} with elements $\langle i | \hat{A} | j \rangle$ can be recognized as a matrix representation of \hat{A} in the basis $|i\rangle$. Reference [45] also proves that Eq. (B1) can be generalized to products of more than two operators, such as

$$\text{Tr}[e^{\Gamma(\hat{A})} e^{\Gamma(\hat{B})} e^{\Gamma(\hat{C})} \dots] = \det(1 + e^{\hat{A}} e^{\hat{B}} e^{\hat{C}} \dots). \quad (\text{B3})$$

In the main text, both of the many-body Hamiltonians \mathcal{H}_i in Eq. (1) and \mathcal{H}_f in Eq. (6) are expressed in a bilinear form that relates with the matrix representation \underline{h}_i and \underline{h}_f of single-particle operators \hat{h}_i and \hat{h}_f , respectively. It will be convenient to work in the eigenbasis of \underline{h}_i , but we will see that the final expression does not depend on such choice of the specific single-particle basis set. The eigenstates of \underline{h}_i are determined by the Bogoliubov transformation

$$a_{\mathbf{k},+}^\dagger = u_{\mathbf{k}} c_{\mathbf{k}}^\dagger - v_{\mathbf{k}} h_{\mathbf{k}}^\dagger, \quad a_{\mathbf{k},-}^\dagger = v_{\mathbf{k}} c_{\mathbf{k}}^\dagger + u_{\mathbf{k}} h_{\mathbf{k}}^\dagger, \quad (\text{B4})$$

with eigenvalue $E_{\mathbf{k},\pm} = \pm \sqrt{\xi_{\mathbf{k}}^2 + \Delta^2}$, where $u_{\mathbf{k}}$ and $v_{\mathbf{k}}$ are the well-known Bogoliubov coefficients defined in Appendix A. For convenience, we also define the corresponding unitary transformation matrix \mathcal{U} , and use a collective subindex $\nu \equiv \{\mathbf{k}, \xi = \pm\}$. With these definitions, and noticing that K_0 and

ω_0 are constant numbers, we arrive at the expressions

$$e^{i\hat{\mathcal{H}}_i t} = e^{iK_0 t} e^{it\Gamma(\hat{h}_i)}, \quad (\text{B5})$$

$$e^{-i\hat{\mathcal{H}}_f t} = e^{-iK_0 t} e^{-i\omega_0 t} e^{-it\Gamma(\hat{h}_f)}, \quad (\text{B6})$$

where

$$\Gamma(\hat{h}_i) = \sum_{\nu,\tau} (\tilde{h}_i)_{\nu\tau} a_\nu^\dagger a_\tau, \quad (\text{B7})$$

$$\Gamma(\hat{h}_f) = \sum_{\nu,\tau} (\tilde{h}_f)_{\nu\tau} a_\nu^\dagger a_\tau. \quad (\text{B8})$$

Here, \tilde{h}_i and \tilde{h}_f are the matrix representation of \hat{h}_i and \hat{h}_f in the eigenstate basis of \underline{h}_i , respectively, which satisfies $\tilde{h}_i = \mathcal{U}^\dagger \underline{h}_i \mathcal{U} = \underline{D}(E_\nu)$ and $\tilde{h}_f = \mathcal{U}^\dagger \underline{h}_f \mathcal{U}$, where $\underline{D}(E_\nu)$ denotes a diagonal matrix with elements E_ν . The initial thermal density matrix $\hat{\rho}_0$ in the same basis can also be written as

$$\hat{\rho}_0 = \frac{1}{\mathcal{Z}} e^{-\Gamma(\hat{\lambda})}, \quad \Gamma(\hat{\lambda}) = \sum_{\nu} \lambda_\nu a_\nu^\dagger a_\nu, \quad (\text{B9})$$

where $e^{-\lambda_\nu} = e^{-E_\nu/k_B T} = n(E_\nu)/[1 - n(E_\nu)]$ and $n(E_\nu) = f(E_\nu) = 1/[e^{E_\nu/k_B T} + 1]$ [68,69]. Here, the normalization constant is given by $\mathcal{Z} = \text{Tr}[\exp(-\sum_{\nu} \lambda_\nu \hat{a}_\nu^\dagger \hat{a}_\nu)] = \det[(1 - \hat{n})^{-1}]$, where $\Gamma(\hat{n}) = \sum_{\nu} n(E_\nu) a_\nu^\dagger a_\nu$.

Finally, we can rewrite Eq. (8) as

$$S(t) = \frac{e^{-i\omega_0 t}}{\mathcal{Z}} \text{Tr}[e^{it\Gamma(\hat{h}_i)} e^{-it\Gamma(\hat{h}_f)} e^{-\Gamma(\hat{\lambda})}], \quad (\text{B10})$$

and according to the trace formula Eq. (B3), we have

$$S(t) = \frac{e^{-i\omega_0 t}}{\mathcal{Z}} \det[1 + e^{it\hat{h}_i} e^{-it\hat{h}_f} e^{-\hat{\lambda}}]. \quad (\text{B11})$$

With the expression of \mathcal{Z} , we arrive at

$$\begin{aligned} S(t) &= e^{-i\omega_0 t} \frac{\det[1 + e^{it\hat{h}_i} e^{-it\hat{h}_f} \hat{n}(1 - \hat{n})^{-1}]}{\det[(1 - \hat{n})^{-1}]} \\ &= e^{-i\omega_0 t} \det[1 - \hat{n} + e^{it\hat{h}_i} e^{-it\hat{h}_f} \hat{n}], \end{aligned} \quad (\text{B12})$$

which is Eq. (10) as promised. Since a determinant remains the same after applying a unitary transformation to any orthogonal set of basis, we can now see that $S(t)$ does not depend on the choice of single-particle basis set. Although, in numerical calculations, it might still be most straightforward to use eigenstates of \underline{h}_i , where \hat{n} and $e^{it\hat{h}_i}$ are both represented by diagonal matrices.

APPENDIX C: NUMERICAL CALCULATIONS

Our numerical calculations are carried out in the coordinate space and limited in the s -wave channel since we assume impurity-medium interactions are dominated by short-range spherical symmetric potentials $V_\sigma(r)$ [3,7]. As mentioned in Appendix B, it would be most convenient to expand the single-particle operators in the eigenbasis of $\underline{h}_i(r)$ in Eq. (13).

To proceed with numerical calculation, we consider a finite system confined in a sphere of large radius R . Keeping k_F constant and carrying out calculation for larger and larger R , we find numerical convergences. In typical calculations, we choose $k_F R = 250\pi - 375\pi$. In our numerical calculation,

we also choose a soft-core van-der-Waals potential given in Eq. (14), which is smooth and nonsingular in the whole coordinate space. On the other hand, this potential have been proved to mimic the interatomic interaction near broad Feshbach resonances very well [70]. This finite-range potential are also characterized by a typical length scale, namely the van-der-Waals length $l_{v\text{dW}}$. In our typical calculations, we choose $k_F l_{v\text{dW}} = 0.01\text{--}0.05$, which are close to realistic values in ultracold experiments. We also find that numerical results are determined by the energy-dependent s -wave scattering length at k_F , and insensitive to other details of $V_\sigma(r)$, such as the value of $l_{v\text{dW}}$ and the number of short-range bound states the potential supported) as long as $k_F l_{v\text{dW}} \ll 1$.

To find the eigenbasis of $h_i(r)$, we discretize the continuous space by expanding the wave function in a fifth-order B-splines basis [71–73]

$$\phi_{v,\sigma}(r) = \sum_n c_n^{(v,\sigma)} b_n(r), \quad (\text{C1})$$

which allows us to use an uneven numerical grid. The soft-core van-der-Waals potential we adopted is relatively deep at the short-range $r \leq l_{v\text{dW}}$, which requires a dense grid. On the other hand, we need to carry out the calculation to large distances $R \gg l_{v\text{dW}}$, where the long-range potentials are very shallow and only requires a sparse grid. Therefore it would be much more efficient to use an uneven numerical grid. We usually use 100–150 grid points at short range $r < 2l_{v\text{dW}}$ and 1000–1500 grid points at large distances. The B-spline basis also allows a higher order approximation of the derivative operator for the calculation of the kinetic energy. However, the B-spline basis are nonorthogonal, therefore, one need to solve a generalized eigenvalue problem,

$$\begin{bmatrix} h_i^{(\uparrow,\uparrow)} & h_i^{(\uparrow,\downarrow)} \\ h_i^{(\downarrow,\uparrow)} & h_i^{(\downarrow,\downarrow)} \end{bmatrix} \begin{pmatrix} \vec{c}^{(v,\uparrow)} \\ \vec{c}^{(v,\downarrow)} \end{pmatrix} = E_v \begin{bmatrix} \underline{S} & 0 \\ 0 & \underline{S} \end{bmatrix} \begin{pmatrix} \vec{c}^{(v,\uparrow)} \\ \vec{c}^{(v,\downarrow)} \end{pmatrix}, \quad (\text{C2})$$

where $\vec{c}^{(v,\sigma)}$ is a vector notation of the coefficients $c_n^{(v,\sigma)}$, and the overlapping matrix \underline{S} have the matrix elements

$$\underline{S}_{mn} = \int dr b_m(r) b_n(r). \quad (\text{C3})$$

The matrix elements of $\underline{h}_i^{(\sigma,\sigma')}$ are given by

$$\underline{h}_i^{(\uparrow,\uparrow)} = -\underline{h}_i^{(\downarrow,\downarrow)} = \frac{1}{2m} \int dr b'_m(r) b'_n(r) - \mu \underline{S}_{mn}, \quad (\text{C4})$$

where the superscript “ \prime ” denotes first derivative and

$$\underline{h}_i^{(\uparrow,\downarrow)} = \underline{h}_i^{(\downarrow,\uparrow)} = \Delta \underline{S}_{mn}. \quad (\text{C5})$$

Similarly, we can diagonalize $\underline{h}_f(r)$ by the expansion

$$\tilde{\phi}_{v,\sigma}(r) = \sum_n d_n^{(v,\sigma)} b_n(r) \quad (\text{C6})$$

and solve the generalized eigenvalue problem

$$\begin{bmatrix} h_f^{(\uparrow,\uparrow)} & h_f^{(\uparrow,\downarrow)} \\ h_f^{(\downarrow,\uparrow)} & h_f^{(\downarrow,\downarrow)} \end{bmatrix} \begin{pmatrix} \vec{d}^{(v,\uparrow)} \\ \vec{d}^{(v,\downarrow)} \end{pmatrix} = \tilde{E}_v \begin{bmatrix} \underline{S} & 0 \\ 0 & \underline{S} \end{bmatrix} \begin{pmatrix} \vec{d}^{(v,\uparrow)} \\ \vec{d}^{(v,\downarrow)} \end{pmatrix}, \quad (\text{C7})$$

where

$$\underline{h}_f^{(\uparrow,\uparrow)} = -\underline{h}_f^{(\downarrow,\downarrow)} = \underline{h}_i^{(\uparrow,\uparrow)} + \int dr b_m(r) V(r) b_n(r) \quad (\text{C8})$$

and

$$\underline{h}_f^{(\uparrow,\downarrow)} = \underline{h}_f^{(\downarrow,\uparrow)} = \underline{h}_i^{(\uparrow,\downarrow)}. \quad (\text{C9})$$

With these eigenvalues and eigenvectors, we can have

$$e^{i\tilde{h}_i t} \rightarrow \underline{D}(e^{iE_v t}), \quad (\text{C10})$$

$$e^{-i\tilde{h}_f t} \rightarrow \underline{\mathcal{U}}^\dagger \underline{D}(e^{-i\tilde{E}_\mu t}) \underline{\mathcal{U}}, \quad (\text{C11})$$

and

$$\hat{n} \rightarrow \underline{D} \left(\frac{1}{e^{E_v/k_B T} + 1} \right), \quad (\text{C12})$$

where \underline{D} denotes a diagonalized matrix. The unitary matrix $\underline{\mathcal{U}}$ has matrix elements

$$\underline{\mathcal{U}}_{\mu\nu} = (\vec{d}^{(\mu,\uparrow)})^\dagger \vec{d}^{(\mu,\downarrow)} \begin{bmatrix} \underline{S} & 0 \\ 0 & \underline{S} \end{bmatrix} \begin{pmatrix} \vec{c}^{(v,\uparrow)} \\ \vec{c}^{(v,\downarrow)} \end{pmatrix}. \quad (\text{C13})$$

If $V_\downarrow(r) \neq 0$, we also need to calculate $\omega_0 = \sum_k \tilde{V}_\downarrow(0)$ arising from the anticommutator in Eq. (4):

$$\begin{aligned} \sum_{\mathbf{k}, \mathbf{q}} \tilde{V}_\downarrow(\mathbf{k} - \mathbf{q}) c_{\mathbf{k}\downarrow}^\dagger c_{\mathbf{q}\downarrow} &= \sum_{\mathbf{k}, \mathbf{q}} \tilde{V}_\downarrow(\mathbf{k} - \mathbf{q}) (c_{\mathbf{q}\downarrow} c_{\mathbf{k}\downarrow}^\dagger - \delta_{\mathbf{k}\mathbf{q}}) \\ &= \sum_{\mathbf{k}, \mathbf{q}} \tilde{V}_\downarrow(\mathbf{k} - \mathbf{q}) h_{\mathbf{q}}^\dagger h_{\mathbf{k}} - \sum_{\mathbf{k}} \tilde{V}_\downarrow(0) \\ &= \sum_{\mathbf{k}, \mathbf{q}} \tilde{V}_\downarrow(\mathbf{k} - \mathbf{q}) h_{\mathbf{k}}^\dagger h_{\mathbf{q}} - \sum_{\mathbf{k}} \tilde{V}_\downarrow(0), \end{aligned} \quad (\text{C14})$$

where we applies the $\tilde{V}_\downarrow(\mathbf{k} - \mathbf{q}) = \tilde{V}_\downarrow(\mathbf{q} - \mathbf{k})$ in the last line, since the interaction potential is assumed to be spherically

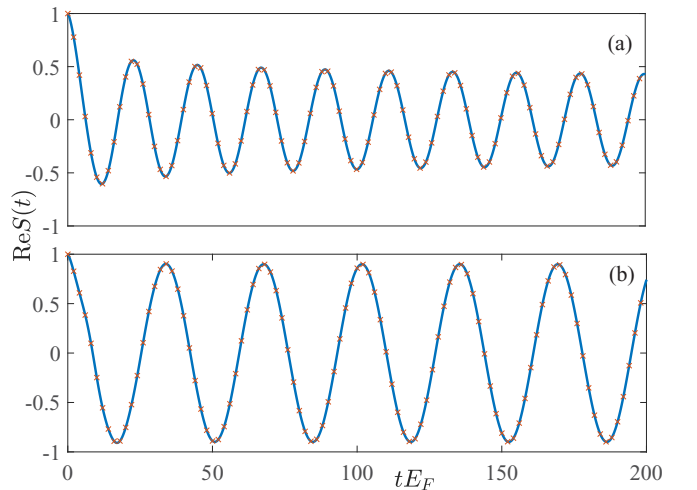


FIG. 9. $S(t)$ at zero temperature for (a) noninteracting Fermi gases as background medium $\Delta = 0$ and (b) BCS superfluid with $k_F a = -2$. The perfectly overlapping blue solid curve and red cross symbols corresponds to $k_F a_\uparrow = -2$, $a_\downarrow = 0$ and $a_\uparrow = 0$, $k_F a_\downarrow = -2$, respectively.

symmetric. Here, we have

$$\begin{aligned}\tilde{V}_\downarrow(\mathbf{k}-\mathbf{q}) &= \langle \mathbf{k} | \hat{V}_\downarrow | \mathbf{q} \rangle = \int d\mathbf{r} \langle \mathbf{k} | \mathbf{r} \rangle V_\downarrow(r) \langle \mathbf{r} | \mathbf{q} \rangle \\ &= \frac{1}{(2\pi)^3} \int d\mathbf{r} V_\downarrow(r) e^{-i(\mathbf{k}-\mathbf{q})\cdot\mathbf{r}}.\end{aligned}\quad (\text{C15})$$

which relates to the Fourier transformation of $V_\downarrow(r)$. We can also express ω_0 as

$$\omega_0 = \sum_{\mathbf{k}} \langle \mathbf{k} | \hat{V}_\downarrow | \mathbf{k} \rangle = \sum_{\mathbf{k}} \int d\mathbf{r} \langle \mathbf{k} | \mathbf{r} \rangle V_\downarrow(r) \langle \mathbf{r} | \mathbf{k} \rangle, \quad (\text{C16})$$

which can be interpreted as taking a trace of the matrix representative of \hat{V}_\downarrow in momentum state basis, and is equivalent to take a trace over any orthogonal basis. In principal, this expression requires summation over infinite \mathbf{k} . However, since we are taking the calculation in a finite system with discretized basis and limited in the s -wave channel, it would be consistent to take the trace over an orthogonal basis $\tilde{b}_m(r)$. Although we cannot directly use the B-spline basis since it is nonorthogonal, we can obtain an orthogonal set by

solving

$$v_\downarrow \vec{g}^m = v_m^\downarrow \underline{S} \vec{g}^m, \quad (\text{C17})$$

where

$$v_{\downarrow mn} = \int dr b_m(r) V_\downarrow(r) b_n(r). \quad (\text{C18})$$

Then we can see that

$$\tilde{b}_m(r) = \sum_n g_n^m b_n(r), \quad (\text{C19})$$

form an orthogonal set of basis and the trace is given by

$$\omega_0 = \sum_m v_m^\downarrow. \quad (\text{C20})$$

With the help of Eqs. (C10), (C11), (C12), and (C20), we can calculate $S(t)$ in Eq. (10) numerically.

One important test is the comparison of $S(t)$ in two cases: (A) $V_\uparrow(r) = V(r)$, $V_\downarrow(r) = 0$ and (B) $V_\uparrow(r) = 0$ and $V_\downarrow(r) = V(r)$. Even though $\omega_0 = 0$ for case (A) but $\omega_0 \neq 0$ for the case (B), the final result of $S(t)$ should nevertheless be exactly the same due to the permutation symmetry between spin states \uparrow and \downarrow , as shown in Fig. 9. The blue solid curve and red cross symbols corresponds to the case (A) and (B), respectively, and they overlap perfectly, for both noninteracting Fermi gases [Fig. 9(a)] and BCS superfluid [Fig. 9(b)].

-
- [1] A. V. Balatsky, I. Vekhter, and J.-X. Zhu, Impurity-induced states in conventional and unconventional superconductors, *Rev. Mod. Phys.* **78**, 373 (2006).
- [2] P. Massignan, M. Zaccanti, and G. M. Bruun, Polarons, dressed molecules and itinerant ferromagnetism in ultra-cold Fermi gases, *Rep. Prog. Phys.* **77**, 034401 (2014).
- [3] R. Schmidt, M. Knap, D. A. Ivanov, J.-S. You, M. Cetina, and E. Demler, Universal many-body response of heavy impurities coupled to a Fermi sea: A review of recent progress, *Rep. Prog. Phys.* **81**, 024401 (2018).
- [4] P. Nozières and C. T. De Dominicis, Singularities in the x-ray absorption and emission of metals. III. One-body theory exact solution, *Phys. Rev.* **178**, 1097 (1969).
- [5] G. D. Mahan, *Many Particle Physics*, 3rd ed. (Kluwer, New York, 2000).
- [6] P. W. Anderson, Infrared Catastrophe in Fermi Gases with Local Scattering Potentials, *Phys. Rev. Lett.* **18**, 1049 (1967).
- [7] M. Knap, A. Shashi, Y. Nishida, A. Imambekov, D. A. Abanin, and E. Demler, Time-Dependent Impurity in Ultracold Fermions: Orthogonality Catastrophe and Beyond, *Phys. Rev. X* **2**, 041020 (2012).
- [8] L. Landau, Über die bewegung der elektronen im kristallgitter, *Phys. Z. Soviet.* **3**, 664 (1933).
- [9] P. M. Chaikin, A. F. Garito, and A. J. Heeger, Excitonic polarons in molecular crystals, *Phys. Rev. B* **5**, 4966 (1972).
- [10] G. Lindemann, R. Lassnig, W. Seidenbusch, and E. Gornik, Cyclotron resonance study of polarons in GaAs, *Phys. Rev. B* **28**, 4693 (1983).
- [11] A. Schirotzek, C.-H. Wu, A. Sommer, and M. W. Zwierlein, Observation of Fermi Polarons in a Tunable Fermi Liquid of Ultracold Atoms, *Phys. Rev. Lett.* **102**, 230402 (2009).
- [12] Y. Zhang, W. Ong, I. Arakelyan, and J. E. Thomas, Polaron-to-Polaron Transitions in the Radio-Frequency Spectrum of a Quasi-Two-Dimensional Fermi Gas, *Phys. Rev. Lett.* **108**, 235302 (2012).
- [13] C. Kohstall, M. Zaccanti, M. Jag, A. Trenkwalder, P. Massignan, G. M. Bruun, F. Schreck, and R. Grimm, Metastability and coherence of repulsive polarons in a strongly interacting Fermi mixture, *Nature (London)* **485**, 615 (2012).
- [14] M. Koschorreck, D. Pertot, E. Vogt, B. Fröhlich, M. Feld, and M. Köhl, Attractive and repulsive Fermi polarons in two dimensions, *Nature (London)* **485**, 619 (2012).
- [15] M. Cetina, M. Jag, R. S. Lous, I. Fritsche, J. T. M. Walraven, R. Grimm, J. Levinsen, M. M. Parish, R. Schmidt, M. Knap, and E. Demler, Ultrafast many-body interferometry of impurities coupled to a Fermi sea, *Science* **354**, 96 (2016).
- [16] M.-G. Hu, M. J. Van de Graaff, D. Kedar, J. P. Corson, E. A. Cornell, and D. S. Jin, Bose Polarons in the Strongly Interacting Regime, *Phys. Rev. Lett.* **117**, 055301 (2016).
- [17] N. B. Jørgensen, L. Wacker, K. T. Skalmstang, M. M. Parish, J. Levinsen, R. S. Christensen, G. M. Bruun, and J. J. Arlt, Observation of Attractive and Repulsive Polarons in a Bose-Einstein Condensate, *Phys. Rev. Lett.* **117**, 055302 (2016).
- [18] F. Scazza, G. Valtolina, P. Massignan, A. Recati, A. Amico, A. Burchianti, C. Fort, M. Inguscio, M. Zaccanti, and G. Roati, Repulsive Fermi Polarons in a Resonant Mixture of Ultracold ^6Li Atoms, *Phys. Rev. Lett.* **118**, 083602 (2017).
- [19] Z. Yan, P. B. Patel, B. Mukherjee, R. J. Fletcher, J. Struck, and M. W. Zwierlein, Boiling a Unitary Fermi Liquid, *Phys. Rev. Lett.* **122**, 093401 (2019).
- [20] Z. Z. Yan, Y. Ni, C. Robens, and M. W. Zwierlein, Bose polarons near quantum criticality, *Science* **368**, 190 (2020).

- [21] G. Ness, C. Shkedrov, Y. Florshaim, O. K. Diessel, J. von Milczewski, R. Schmidt, and Y. Sagi, Observation of a Smooth Polaron-Molecule Transition in a Degenerate Fermi Gas, *Phys. Rev. X* **10**, 041019 (2020).
- [22] F. Chevy, Universal phase diagram of a strongly interacting Fermi gas with unbalanced spin populations, *Phys. Rev. A* **74**, 063628 (2006).
- [23] C. Lobo, A. Recati, S. Giorgini, and S. Stringari, Normal State of a Polarized Fermi Gas at Unitarity, *Phys. Rev. Lett.* **97**, 200403 (2006).
- [24] R. Combescot, A. Recati, C. Lobo, and F. Chevy, Normal State of Highly Polarized Fermi Gases: Simple Many-Body Approaches, *Phys. Rev. Lett.* **98**, 180402 (2007).
- [25] M. Punk, P. T. Dumitrescu, and W. Zwerger, Polaron-to-molecule transition in a strongly imbalanced Fermi gas, *Phys. Rev. A* **80**, 053605 (2009).
- [26] X. Cui and H. Zhai, Stability of a fully magnetized ferromagnetic state in repulsively interacting ultracold Fermi gases, *Phys. Rev. A* **81**, 041602(R) (2010).
- [27] C. J. M. Mathy, M. M. Parish, and D. A. Huse, Trimers, Molecules, and Polarons in Mass-Imbalanced Atomic Fermi Gases, *Phys. Rev. Lett.* **106**, 166404 (2011).
- [28] R. Schmidt, T. Enss, V. Pietilä, and E. Demler, Fermi polarons in two dimensions, *Phys. Rev. A* **85**, 021602(R) (2012).
- [29] S. P. Rath and R. Schmidt, Field-theoretical study of the Bose polaron, *Phys. Rev. A* **88**, 053632 (2013).
- [30] A. Shashi, F. Grusdt, D. A. Abanin, and E. Demler, Radio-frequency spectroscopy of polarons in ultracold Bose gases, *Phys. Rev. A* **89**, 053617 (2014).
- [31] W. Li and S. Das Sarma, Variational study of polarons in Bose-Einstein condensates, *Phys. Rev. A* **90**, 013618 (2014).
- [32] P. Kroiss and L. Pollet, Diagrammatic Monte Carlo study of a mass-imbalanced Fermi-polaron system, *Phys. Rev. B* **91**, 144507 (2015).
- [33] J. Levinsen, M. M. Parish, and G. M. Bruun, Impurity in a Bose-Einstein Condensate and the Efimov Effect, *Phys. Rev. Lett.* **115**, 125302 (2015).
- [34] H. Hu, A.-B. Wang, S. Yi, and X.-J. Liu, Fermi polaron in a one-dimensional quasiperiodic optical lattice: The simplest many-body localization challenge, *Phys. Rev. A* **93**, 053601 (2016).
- [35] O. Goulko, A. S. Mishchenko, N. Prokof'ev, and B. Svistunov, Dark continuum in the spectral function of the resonant Fermi polaron, *Phys. Rev. A* **94**, 051605(R) (2016).
- [36] H. Hu, B. C. Mulkerin, J. Wang, and X.-J. Liu, Attractive Fermi polarons at nonzero temperatures with a finite impurity concentration, *Phys. Rev. A* **98**, 013626 (2018).
- [37] B. C. Mulkerin, X.-J. Liu, and H. Hu, Breakdown of the Fermi polaron description near Fermi degeneracy at unitarity, *Ann. Phys.* **407**, 29 (2019).
- [38] J. Wang, X.-J. Liu, and H. Hu, Roton-Induced Bose Polaron in the Presence of Synthetic Spin-Orbit Coupling, *Phys. Rev. Lett.* **123**, 213401 (2019).
- [39] F. Isaule, I. Morera, P. Massignan, and B. Juliá-Díaz, Renormalization-group study of Bose polarons, *Phys. Rev. A* **104**, 023317 (2021).
- [40] I. Bloch, J. Dalibard, and W. Zwerger, Many-body physics with ultracold gases, *Rev. Mod. Phys.* **80**, 885 (2008).
- [41] C. Chin, R. Grimm, P. Julienne, and E. Tiesinga, Feshbach resonances in ultracold gases, *Rev. Mod. Phys.* **82**, 1225 (2010).
- [42] U. Weiss, *Quantum Dissipative Systems* (World Scientific, Singapore, 1999), Vol. 10.
- [43] A. Rosch, Quantum-coherent transport of a heavy particle in a fermionic bath, *Adv. Phys.* **48**, 295 (1999).
- [44] L. S. Levitov and H. Lee, Electron counting statistics and coherent states of electric current, *J. Math. Phys.* **37**, 4845 (1996).
- [45] I. Klich, *Full Counting Statistics: An Elementary Derivation of Levitov's Formula* (Kluwer, Dordrecht, 2003).
- [46] K. Schönhammer, Full counting statistics for noninteracting fermions: Exact results and the Levitov-Lesovik formula, *Phys. Rev. B* **75**, 205329 (2007).
- [47] D. A. Ivanov and A. G. Abanov, Fisher-Hartwig expansion for Toeplitz determinants and the spectrum of a single-particle reduced density matrix for one-dimensional free fermions, *J. Phys. A: Math. Theor.* **46**, 375005 (2013).
- [48] J. Wang, X.-J. Liu, and H. Hu, Exact Quasiparticle Properties of a Heavy Polaron in BCS Fermi Superfluids, *Phys. Rev. Lett.* **128**, 175301 (2022).
- [49] A. J. Leggett, Cooper pairing in spin-polarized Fermi systems, *J. Phys. (Paris)* **42**, C7 (1980).
- [50] P. Nozières and S. Schmitt-Rink, Bose condensation in an attractive fermion gas: From weak to strong coupling superconductivity, *J. Low Temp. Phys.* **59**, 195 (1985).
- [51] H. Hu, X.-J. Liu, and P. D. Drummond, Equation of state of a superfluid Fermi gas in the BCS-BEC crossover, *Europhys. Lett.* **74**, 574 (2006).
- [52] Y. Nishida, Polaronic Atom-Trimer Continuity in Three-Component Fermi Gases, *Phys. Rev. Lett.* **114**, 115302 (2015).
- [53] W. Yi and X. Cui, Polarons in ultracold Fermi superfluids, *Phys. Rev. A* **92**, 013620 (2015).
- [54] M. Pierce, X. Leyronas, and F. Chevy, Few Versus Many-Body Physics of an Impurity Immersed in a Superfluid of Spin 1/2 Attractive Fermions, *Phys. Rev. Lett.* **123**, 080403 (2019).
- [55] H. Hu, J. Wang, J. Zhou, and X.-J. Liu, Crossover polarons in a strongly interacting Fermi superfluid, *Phys. Rev. A* **105**, 023317 (2022).
- [56] A. Bigué, F. Chevy, and X. Leyronas, Mean-field vs RPA calculation of the energy of an impurity immersed in a spin 1/2 superfluid, *Phys. Rev. A* **105**, 033314 (2022).
- [57] Y. Luh, Bound state in superconductors with paramagnetic impurities, *Acta Phys. Sin.* **21**, 75 (1965).
- [58] H. Shiba, Classical spin in superconductors, *Prog. Theor. Phys.* **40**, 435 (1968).
- [59] A. I. Rusinov, Superconductivity near a paramagnetic impurity, *JETP Lett. (USSR)* **9**, 85 (1969).
- [60] E. Vernier, D. Pekker, M. W. Zwierlein, and E. Demler, Bound states of a localized magnetic impurity in a superfluid of paired ultracold fermions, *Phys. Rev. A* **83**, 033619 (2011).
- [61] L. Jiang, L. O. Baksmaty, H. Hu, Y. Chen, and H. Pu, Single impurity in ultracold Fermi superfluids, *Phys. Rev. A* **83**, 061604(R) (2011).
- [62] I. Ferrier-Barbut, M. Delehay, S. Laurent, A. T. Grier, M. Pierce, B. S. Rem, F. Chevy, and C. Salomon, A mixture of Bose and Fermi superfluids, *Science* **345**, 1035 (2014).
- [63] X.-C. Yao, H.-Z. Chen, Y.-P. Wu, X.-P. Liu, X.-Q. Wang, X. Jiang, Y. Deng, Y.-A. Chen, and J.-W. Pan, Observation of Coupled Vortex Lattices in a Mass-Imbalance Bose and Fermi Superfluid Mixture, *Phys. Rev. Lett.* **117**, 145301 (2016).

- [64] R. Roy, A. Green, R. Bowler, and S. Gupta, Two-Element Mixture of Bose and Fermi Superfluids, *Phys. Rev. Lett.* **118**, 055301 (2017).
- [65] S.-K. Tung, C. Parker, J. Johansen, C. Chin, Y. Wang, and P. S. Julienne, Ultracold mixtures of atomic ^6Li and ^{133}Cs with tunable interactions, *Phys. Rev. A* **87**, 010702(R) (2013).
- [66] F. Schäfer, N. Mizukami, and Y. Takahashi, Feshbach resonances of large-mass-imbalance Er-Li mixtures, *Phys. Rev. A* **105**, 012816 (2022).
- [67] V. Gurarie and L. Radzihovsky, Resonantly-paired fermionic superfluids, *Ann. Phys.* **322**, 2 (2007).
- [68] D. A. Abanin and L. S. Levitov, Tunable Fermi-Edge Resonance in an Open Quantum Dot, *Phys. Rev. Lett.* **93**, 126802 (2004).
- [69] D. A. Abanin and L. S. Levitov, Fermi-Edge Resonance and Tunneling in Nonequilibrium Electron Gas, *Phys. Rev. Lett.* **94**, 186803 (2005).
- [70] J. Wang, J. P. D’Incao, B. D. Esry, and C. H. Greene, Origin of the Three-Body Parameter Universality in Efimov Physics, *Phys. Rev. Lett.* **108**, 263001 (2012).
- [71] C. de Boor, *A Practical Guide to Splines* (Springer, New York, 1978).
- [72] H. W. van der Hart, B-spline methods in R-matrix theory for scattering in two-electron systems, *J. Phys. B: At. Mol. Opt. Phys.* **30**, 453 (1997).
- [73] J. Wang and C. H. Greene, Quantum-defect analysis of $3p$ and $3dH_3$ Rydberg energy levels, *Phys. Rev. A* **82**, 022506 (2010).